J. Phys. D: Appl. Phys. **46** (2013) 125304 (9pp) doi:10.1088/0022-3727/46/12/125304

Negative capacitance in (FeCoZr)–(PZT) nanocomposite films

T N Kołtunowicz[1], J A Fedotova[2], P Zhukowski[1], A Saad[3], A Fedotov[4], J V Kasiuk[2] and A V Larkin[4]

[1] Department of Electrical Devices and High Voltages Technologies, Lublin University of Technology, Nadbystrzycka 38a, 20-618 Lublin, Poland
[2] National Centre for Particles and High Energy Physics of Belarusian State University, Bogdanovich 153, 220040 Minsk, Belarus
[3] Department of Applied Sciences, Al-Balqa Applied University, PO Box 2041, Amman 11953, Salt, Jordan
[4] Department of Energophysics, Belarusian State University, Independence av. 4, 220030, Minsk, Belarus

E-mail: t.koltunowicz@pollub.pl

Received 7 October 2012, in final form 24 December 2012
Published 21 February 2013
Online at stacks.iop.org/JPhysD/46/125304

Abstract
In this work, attention was focused on the inductive contribution to the real part of admittance $G(T, f)$ in $(Fe_{0.45}Co_{0.45}Zr_{0.10})_x(PZT)_{(1-x)}$ nanocomposite films deposited in a mixed argon–oxygen atmosphere. The observed $G(x, f, T)$ dependences for the films on the dielectric side of the insulator–metal transition demonstrated the negative capacitance (NC) effect that was maximal for the nanocomposites with $0.40 < x < 0.60$, where the metallic FeCoZr nanoparticles were totally oxidized. The NC effect was explained by a specially developed model for the ac hopping conductance of the electrons between the fully oxidized nanoparticles embedded in the PZT matrix. In accordance with the model, under the determined conditions the observed structure of nanocomposites led to an increase in the hopping electron mean lifetime on nanoparticles and hence to the possibility of positive angles of the phase shifts θ and a proper NC (inductive-like contribution) effect.

(Some figures may appear in colour only in the online journal)

1. Introduction

In the last decade, the design and fabrication of multifunctional nanostructured and nanocomposite materials have attracted considerable attention [1–3]. In contrast to their more limited single-component counterparts, nanocomposite materials offer enhanced functionality and multifunctional properties.

The nanocomposites made from metal nanoparticles (NPs) in dielectric matrixes are of great interest due to their potential applications in plasmonics [2], data processing [1, 2], shielding of high-frequency electromagnetic fields [3], in microwave communication devices and their miniaturization [3], etc. Low-loss nanocomposites with improved magneto-dielectric properties at radio frequencies (1 MHz–1 GHz) can be fabricated on the basis of nanocomposites with the so-called 'core/shell' nanostructures of NPs when iron-cobalt-based NPs are surrounded by their own oxides and embedded in the dielectric (alumina, silica, PZT, polymeric, etc) matrix [3]. Such materials featuring high values of magnetic permeability (μ) and dielectric permittivity (ε) are promising for various advanced applications. In addition, their 'core/shell' nanostructure may exhibit dual physical properties of 'core' and 'shell' materials [4]. Fabrication of lightweight and volume-efficient electrical components using such nanocomposites is one of the major research problems in the passive component sector using embedded technologies [5, 6]. For instance, the high-ε dielectric matrix in nanocomposites is useful for filtering, bypassing and shielding aimed at noise suppression in high-speed electronics.

One of the most interesting effects, quite often exhibited in metal–dielectric nanocomposites which can be used for the production of passive electric components, is the so-called negative capacitance (NC) [7–11]. Apart from nanocomposites, the phenomenon of NC, observed also in some other materials and devices, corresponds to the inductive contribution to admittance (impedance). The NC effect in a low-frequency range (for $f < 1$ MHz) has been reported for a variety of disordered and inhomogeneous metal–semiconductor systems, e.g. doped boric oxide glass [12], GaAs quantum well infrared photodetectors [13], GaAs n–i–p

structures [14], GaAs homojunction photodetectors [15], glassy alloys of Ga_xTe_{100-x} [16], hydrogenated amorphous silicon diodes [17], etc.

Although the physical origin of NC has been discussed in the literature (see [7, 18–22] and references therein), the concept of NC is still not widely recognized. The microscopic physical mechanisms associated with NC were differing considerably in these works and were dependent on the material features or on the particular device studied. In some of them the appearance of the NC effect was attributed to the influence of the metal–semiconductor interface (see [22]), e.g. trapping processes, charge carrier capture and emission, space charge effect or contact injection. The NC phenomenon in [18–20] was interpreted to be proceeding from the purely electrostatic charge redistribution within the nanostructures (devices) or inhomogeneous material and explained with reference to impact ionization, injection of minority carriers or the imaginary component of carrier mobility. Some theories have been based on Drude's model [19] as well as space charge limited conduction [22] to explain the NC effect in disordered solids having energy distributed trap states (see also [21]). In [20] the Drude model was correlated with a simple resistor–capacitor equivalent circuit model explaining the NC effect.

In our works [7–11], the presence of NC in metal–dielectric FeCoZr–alumina nanocomposite films was attributed to the inhomogeneous distribution of the electron routes due to either the hopping mechanism of the carrier transport (below the percolation threshold x_C) or a complicated motion of the electrons by a percolation net of electrically contacted metallic NPs (beyond the x_C). This resulted in the formation of coil-like current routes in the samples studied, making an inductive-like contribution to admittance [8–11]. Such behaviour enabled one to consider a nanocomposite as a system of nano-coils embedded in the dielectric matrix. This electric behaviour of nanocomposites makes it possible to use them as non-coil-like (planar) miniaturized inductive elements in electronic circuits with a giant equivalent inductance $L \approx 20\ \mu$H per cubic micrometre (see [10, 23]).

The NC effect observed in [7–11] in the metal–dielectric nanocomposite films $(Fe_{0.45}Co_{0.45}Zr_{0.10})_x(Al_2O_3)_{(1-x)}$ was very weak in the samples deposited in an atmosphere of pure Ar gas but it was strongly enhanced after the incorporation of oxygen into the vacuum chamber [24], where the 'core/shell' nanostructure was realized, as has been demonstrated in [25]. Also, it should be noted that in most of the as-deposited (non-annealed) FeCoZr–Al_2O_3 nanocomposite samples the NC effect was observed only below 120–150 K, which is not convenient for applications in electronics and electric engineering. As shown in [25], the additional annealing procedure resulted in an increase in the fraction of FeCo-based oxide 'shells' around the metallic NPs' 'cores' and an enhancement of the NC effect. Moreover, it shifted to the region of room temperature and was observed over a wider range of frequencies [26]. The performed experiments indicated that, to enhance the NC effect, it is needed to increase the volume of the FeCo-based oxide 'shells' (ideal to oxidize NPs completely) in nanocomposite films on the dielectric side of the insulator–metal transition (IMT), i.e. below the percolation threshold x_C [27]. As shown in [25, 28], a dense coat of alumina formed around metallic NPs during the nanocomposite film deposition that prevented their complete oxidation. At the same time, replacement of the alumina matrix on PZT, as was indicated in [26, 29, 30], resulted in complete oxidation of FeCoZr NPs when x was lower than a value of x_C.

So, the main goal of this paper is to study the NC effect in the as-deposited (non-annealed) nanocomposite samples containing oxidized FeCoZr NPs embedded in more high-ohmic PZT (=Pb(ZrTi)O_3) as a dielectric matrix. PZT in the studied nanocomposite films was selected due to two of its peculiarities not observed in alumina. Firstly, PZT is a less corrosion resistant material than alumina allowing one to hope to get a much greater portion of the oxidized metallic fraction in $(FeCoZr)_x(PZT)_{(1-x)}$ films. Secondly, PZT retains the ferroelectric and piezoelectric properties in the crystalline state permitting one to expand the possibilities of tuning the magnetic and electric properties of nanocomposites. For example, some of the composite and multilayered materials containing PZT and magnetic fractions (Co-, Fe-, Ni-based alloys, $CoFe_2O$, $NiFe_2O$, $CoFe_2O_4$, etc) exhibit the magnetoelectric effects associated with the appearance of electric polarization under an external magnetic field or, on the contrary, the appearance of magnetization when an electric field is applied [31, 32]. The possibility of using these phenomena for manufacturing of sensors, modulators, waveguides, high-speed switches and phase inverters was considered in [32, 33].

2. Experimental

In our experiments we used $(Fe_{0.45}Co_{0.45}Zr_{0.10})_x(PZT)_{(1-x)}$ films with $0.35 < x < 0.88$ deposited by ion-beam sputtering of a complex target in a chamber evacuated with a mixture of Ar and O_2 under partial pressures $P_{Ar} = 6.7$ mPa and $P_{O_2} = 3.2$ mPa, respectively.

All the technological procedures and experimental techniques were described earlier in [26, 29, 30]. The compound target to be sputtered consisted of the $Fe_{0.45}Co_{0.45}Zr_{0.10}$ alloy plate measuring 280×80 mm^2, with some doped PZT stripes 8 mm in width arranged on its surface. Irregular distribution of PZT stripes (with continuously increasing space between them) at the target surface produced a wide range of values for the metal-to-dielectric ratio x (depending on the mutual arrangement of the target and substrates) in one technological cycle.

The studied samples (films) were sputtered at temperature ≈373 K onto glass–ceramic substrates for electric measurements and on thin aluminum foils for Mössbauer investigations. The thickness of the composite films was ranging from 1 to 2 μm; the ceramic substrate with the deposited films was 250 mm long, 50 mm wide and 0.6 mm thick. The content of chemical elements in the composites was measured using special micro-probe x-ray analyses in a scanning electron microscope (SEM) LEO 1455VP accurate to ∼1%. The thickness of the films was measured by SEM accurate up to ∼2–3% on cleavages of the samples studied.

The phase composition and local atomic ordering in the FeCoZr NPs were investigated in detail using the Mössbauer and Raman spectroscopy methods as reported in [29, 30]. The chemical composition of the studied samples was additionally verified by the Rutherford backscattering method (RBS) [29]. In addition, the structure of the as-deposited FeCoZr–alumina composites was investigated using transmission (TEM) and scanning (SEM) electron microscopes [25].

The as-deposited films were cut to give rectangular samples (10 mm long and 2 mm wide) on which four electrical probes were prepared using a special silver paste. Measurements of the admittance $G(f, T)$ of the studied samples were performed in a cryostat with a special PC-based control system at measuring temperatures T varying from 80 K to 373 K in steps of 5 K. In a set-up for $G(f, T)$ measurements either a precision HIOKI 3532 LCR HiTESTER ac bridge (for the frequency range 50 Hz–100 kHz) or a precision Hewlett Packard LCR-meter HP 4284A (for measurements at frequencies 100 kHz–10 MHz) was used. During the experiments, the changes in the full resistance and phase of the samples studied were fixed to calculate the real and imaginary parts of admittance. In more detail this procedure was described in [34–36]. The absolute values of admittance were measured accurate up to ~4%, whereas a specific admittance was measured to accuracy not higher than 10% due to errors in the measured thicknesses and distances between the potential probes in the samples studied.

3. Results and discussion

3.1. Phase composition

The phase composition of the $(FeCoZr)_x(PZT)_{1-x}$ films sintered in Ar+O_2 atmosphere was identified based on the room-temperature Mössbauer spectra shown in figure 1. These spectra revealed a sequential transition from non-magnetic spectra at $x < 0.67$ towards ferromagnetically split spectra with increase in x. Spectra of the films with $x < 0.67$ (see $(FeCoZr)_{0.35}(PZT)_{0.65}$ and $(FeCoZr)_{0.50}(PZT)_{0.50}$ in figure 1) were fitted with two doublets D_1 ($\delta = 0.32$ (0.35) mm s^{-1}, $\Delta = 0.96$ (0.91) mm s^{-1}) and D_2 ($\delta = 0.96$ (0.91) mm s^{-1}, $\Delta = 1.72$ mm s^{-1}). Hyperfine parameters of these spectra correspond to Fe^{3+} and Fe^{2+}, respectively, so that they could be identified as a superposition of superparamagnetic NPs of the maghemite γ-Fe_2O_3 and/or magnetite Fe_3O_4 (Fe^{3+}) and a wüstite-based phase $(Fe_xCo_{1-x})_{1-\delta}O$ (Fe^{2+}). It is noteworthy that no contribution of non-oxidized α-FeCo(Zr,O) could be fitted in these spectra as was in the case of the oxidized FeCoZr–Al_2O_3 films for $x \leqslant 0.54$ [25]. The fully oxidized status of NPs for $x < 0.67$ is also supported by extended x-ray absorption fine structure (EXAFS) and x-ray diffraction (XRD) results (to be published elsewhere). The tendency for increase in $(Fe_xCo_{1-x})_{1-\delta}O$ contribution with respect to γ-Fe_2O_3 and/or $Fe_3O_4$is demonstrated by the relationship between Fe^{2+} and Fe^{3+} fractions in fitted Mössbauer spectra, i.e. 89/11 for $x = 0.35$, 80/20 for $x = 0.50$ and 46/36 for $x = 0.67$ (see figure 1). Granular films with $x \geqslant 0.67$ reveal

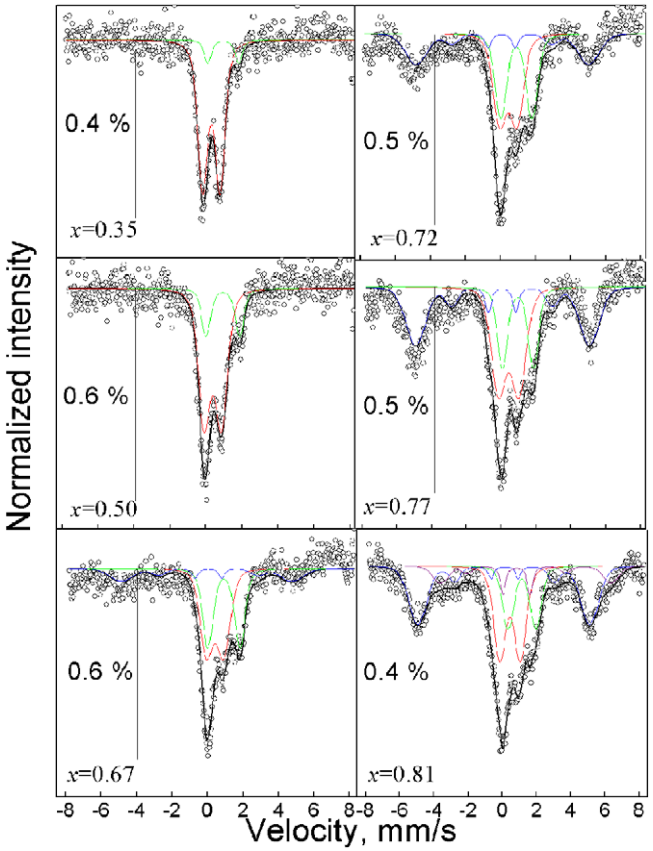

Figure 1. Experimental (points) and fitted (envelope) Mössbauer spectra of the $(FeCoZr)_x(PZT)_{1-x}$ granular films ($0.35 \leqslant x \leqslant 0.81$) recorded at room temperature. The spectra were fitted with Fe^{3+} doublet (red curve), Fe^{2+} doublet (green curve) and superposition of two magnetic sextets (blue curves) corresponding to the α-FeCo alloy.

spectra with a ferromagnetically split subspectrum ($H_{hf} \approx 30$–31 T) corresponding to α-FeCo(Zr) agglomerations whose contribution increases with x.

From figure 1 and from our previous paper [25] it may be concluded that at low concentrations of metallic NPs an increase in their oxidation and growth of $(Fe_xCo_{1-x})_{1-\delta}O$ (Fe^{2+}) contribution below $x = 0.40$ is observed, whereas the dominating Fe_3O_4 (Fe^{3+}) phase is observed at $x > 0.50$ with growing x.

3.2. Admittance

During our previous studies of the real part of admittance $G(f, T)$ in metal–dielectric nanocomposites we found that the NC effect (inductive-like contribution to G) in $(Fe_{0.45}Co_{0.45}Zr_{0.10})_x(Al_2O_3)_{1-x}$ nanocomposites was very weak for the as-deposited samples [7–11], being increased in the films deposited in a mixed argon–oxygen gas atmosphere, especially after high-temperature annealing [24]. In doing so, the composition/frequency/temperature dependences $G(x, f, T)$ of the real part of admittance in the films $(Fe_{0.45}Co_{0.45}Zr_{0.10})_x(Al_2O_3)_{1-x}$, deposited in mixed Ar + O_2, displayed IMT with increasing metallic fraction content x. This was manifested as a change in sign for $dG(T)/dT$ from negative to positive when crossing x close to $x_C \approx 0.55$.

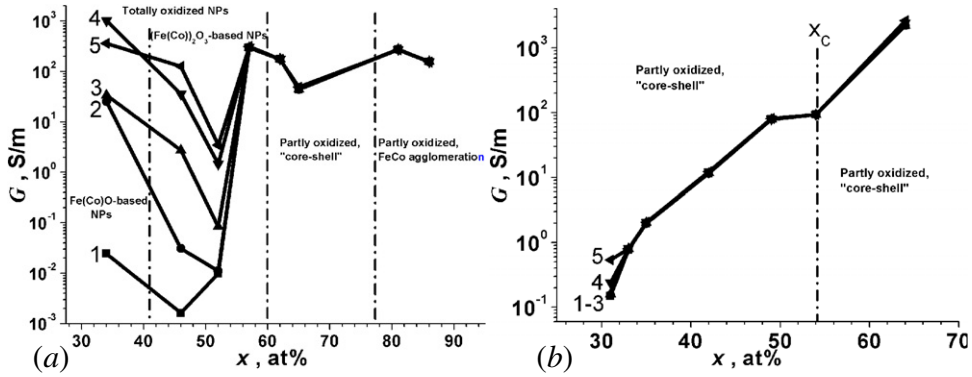

Figure 2. Dependences of the real part of admittance for the nanocomposite films (*a*) $(Fe_{0.45}Co_{0.45}Zr_{0.10})_x(PZT)_{1-x}$ and (*b*) $(Fe_{0.45}Co_{0.45}Zr_{0.10})_x(Al_2O_3)_{1-x}$ deposited in a mixed argon–oxygen atmosphere at $P_{O_2} = 3.2$ mPà, at frequencies $f = 1.5$ kHz (1), 10 kHz (2), 100 kHz (3), 500 kHz (4), 1000 kHz (5) and measurement temperature $T = 300$ K.

As follows from the experiments described in this paper, the concentration $G(x)$ and temperature $G(T)$ dependences in the studied films $(Fe_{0.45}Co_{0.45}Zr_{0.10})_x(PZT)_{1-x}$ and in $(FeCoZr)_x(Al_2O_3)_{1-x}$ [7–11] really display the transition from low-conductive (insulating) to highly conductive (metallic-like) state with increasing x(figure 2). At the same time, as follows from the experiments presented, $G(x, f)$ dependences in the $(FeCoZr)_x(PZT)_{1-x}$ films show principally different behaviour with respect to $(Fe_{0.45}Co_{0.45}Zr_{0.10})_x(Al_2O_3)_{1-x}$ nanocomposites. We shall try to link these features of $G(x, f)$ curves to the peculiarities of NPs' structure in the nanocomposites under study, which are indicated in figure 2 for different regions of x values.

First, the difference is in a non-monotonic change of $G(x)$ dependences measured at room temperature in the $(Fe_{0.45}Co_{0.45}Zr_{0.10})_x(PZT)_{1-x}$ nanocomposites (figure 2(*a*)) as compared with a monotonic increase for the $(Fe_{0.45}Co_{0.45}Zr_{0.10})_x(Al_2O_3)_{1-x}$ films (figure 2(*b*)). As is seen from figure 2(*a*), the curves for $G(x)$ on G-scale (at least at low frequencies) are lower by 1–2 orders of magnitude in the case of $(Fe_{0.45}Co_{0.45}Zr_{0.10})_x(PZT)_{1-x}$ samples compared with the $(Fe_{0.45}Co_{0.45}Zr_{0.10})_x(Al_2O_3)_{1-x}$ films. This is indicative of a higher content of the oxide phase in the samples of $(Fe_{0.45}Co_{0.45}Zr_{0.10})_x(PZT)_{1-x}$ that was confirmed by Mössbauer and Raman spectroscopy in [26, 29, 30] and discussed in section 3.1 of this paper.

Second, $G(x)$ dependences for $(Fe_{0.45}Co_{0.45}Zr_{0.10})_x(PZT)_{1-x}$ display two dramatic changes in their progress with increasing NP concentration: (i) they approach a minimum at low values when $x \approx x_{min}$ and (ii) there is a transition from a sharp increase (by 5–6 orders) beyond this minimum to a much smaller change (practically saturation) of $G(x)$ with x. Note also that the position of x_{min} on $G(x)$ curves is shifted from $x = 0.46$ to $x = 0.52$ as the measuring frequency increases, whereas saturation occurs at some critical value $x_C \approx 0.56$ after which $G(x)$ values hardly change with the NP content, being also independent of the frequency. Taking into account the increase in the oxide fraction with x revealed in [26, 28, 29, 30] (the same but to a lesser degree was observed in the $(Fe_{0.45}Co_{0.45}Zr_{0.10})_x(Al_2O_3)_{1-x}$ films [26, 28]) and the behaviour of $G(f, T)$ curves shown in [37] as well as the temperature dependences of dc resistance observed in [7], we can attribute the value of x_C to the concentration associated with a direct electric contact of the fully oxidized FeCo-based oxide NPs. Note that the observed value of x_C lies at a position slightly higher than the percolation threshold position (∼0.5) predicted by percolation theory [27] for three-dimensional percolating systems. The independence of $G(x)$ of the frequency beyond the percolation threshold $x_C \approx 0.56$ is similar to the behaviour of the same curves for the $(Fe_{0.45}Co_{0.45}Zr_{0.10})_x(Al_2O_3)_{1-x}$ nanocomposite films [7, 28] also deposited in an oxygen-containing atmosphere at $x > 0.55$. Moreover, this confirms the formation of a high-conduction percolation net of oxidized metallic NPs or agglomerations of oxidized and metallic NPs within the dielectric PZT matrix.

A minimum in $G(x)$ dependences found at low x should be considered with due regards for a series of phase transformations in the studied nanocomposites, described in section 3.1 of this paper and in [26, 29, 30, 37] for the films deposited in an Ar + O_2 atmosphere at different partial pressures of oxygen $P_{O_2} = 2.4$–3.2 mPa. In particular, as shown above, an increase in the oxide fraction of NPs with growing x was revealed for the $(Fe_{0.45}Co_{0.45}Zr_{0.10})_x(PZT)_{1-x}$ films by Mössbauer spectroscopy and EXAFS. Moreover, at $x < x_{min}$ these oxides contained mainly FeO-based NPs (their concentration increasing as $x \to x_{mib}$), whereas at $x_{min} < x < x_C$ Fe_2O_3-based oxide was dominant. This enables one to assume that the minima of $G(x)$ curves in figure 2(*a*) at low x can be due to the concurrent growth of FeO-based NPs (as is known, FeO is an insulator) when x is increased and that there is a tendency for the formation of a less resistive (semiconducting) net from Fe_2O_3-based oxide NPs at $x > x_{min}$ up to the percolation threshold. Note that, in spite of the progressive oxidation of NPs in the alumina matrix observed in [27] and despite the formation of their 'core–shell' structure, FeCoZr–Al_2O_3 nanocomposites do not display full oxidation of NPs for any region of x values (see figure 2(*b*)). This is probably connected with the much higher chemical inertness of alumina NPs, which cover the metallic NPs by a tighter (as compared with PZT) passivating shell during the deposition process, hindering penetration of oxygen ions from the deposition atmosphere into the metallic NPs.

The third characteristic feature distinguishing the behaviour of $(Fe_{0.45}Co_{0.45}Zr_{0.10})_x(PZT)_{1-x}$ and $(Fe_{0.45}Co_{0.45}$

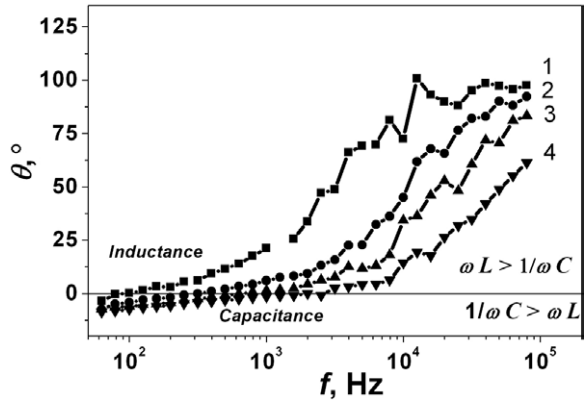

Figure 3. $\theta(f)$ curves for the as-deposited sample $(Fe_{0.45}Co_{0.45}Zr_{0.10})_{0.42}(PZT)_{0.58}$. Measuring temperatures: (1)—243 K, (2)—263 K, (3)—283 K, (4)—303 K.

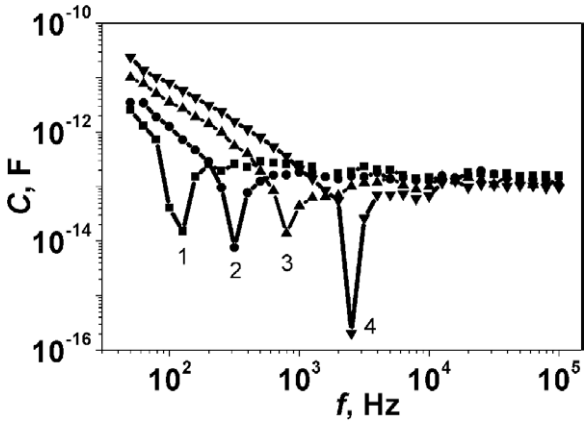

Figure 4. Module $|C|(f)$ curves for the as-deposited sample $(Fe_{0.45}Co_{0.45}Zr_{0.10})_{0.42}(PZT)_{0.58}$. Measuring temperatures: (1)—243 K, (2)—263 K, (3)—283 K, (4)—303 K.

$Zr_{0.10})_x(Al_2O_3)_{1-x}$ nanocomposite films on the dielectric side of the IMT is associated with different frequency and temperature dependences of the observed NC effect. Note also that for the $(Fe_{0.45}Co_{0.45}Zr_{0.10})_x(PZT)_{1-x}$ samples a maximal NC effect was observed in the most high-ohmic films around x_{min} (see figure 2(*a*)). Therefore, in what follows, attention will be focused only on the description of results obtained for the most high-ohmic sample of $(Fe_{0.45}Co_{0.45}Zr_{0.10})_{0.42}(PZT)_{0.58}$ that exhibited a maximal NC effect.

As was observed in [24, 26], for the $(Fe_{0.45}Co_{0.45}Zr_{0.10})_x(Al_2O_3)_{1-x}$ samples the NC effect corresponding to positive values of the phase-angle shift $\theta(f)$ was observed only at temperatures lower than 120 K in the as-deposited state, shifting to room temperature and higher frequencies after the special heat treatment. At the same time, as illustrated in figure 3, the $(Fe_{0.45}Co_{0.45}Zr_{0.10})_x(PZT)_{(1-x)}$ nanocomposite films around x_{min} value displayed large positive shifts of the phase angle θ, approaching +90° at $f > 10^4$ Hz and at $T > 240$ K even in the as-deposited state. This confirms that the NC effect is progressively enhanced in nanocomposites containing fully oxidized NPs.

As shown in figure 3, $\theta(f)$ curves for the as-deposited sample with $x = 0.42$ change their sign from negative to positive, displaying the inductive-like behaviour at higher

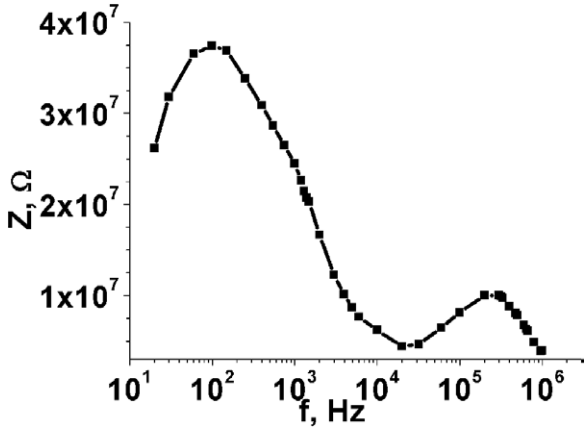

Figure 5. Frequency dependence of full impedance $Z$for the as-deposited sample $(Fe_{0.45}Co_{0.45}Zr_{0.10})_{0.42}(PZT)_{0.58}$ measured at $T = 303$ K.

temperatures (243–303 K). For comparison, figure 4 presents the frequency dependence of the capacitive contribution (its modulus) to the reactive part of admittance for the same sample whose $\theta(f)$ curves are given in figure 3.

Let us correlate the behaviour of the curves for $\theta(f)$ and $|C|(f)$ shown in figures 3 and 4. As seen, the modulus of $|C|(f)$ dependences in the low-f range fall down as f increases, approaching their minima at some critical frequency f_{min}. The values of f_{min} coincide with the frequencies where the curves for $\theta(f)$ cross the zero line (changing their sign from negative to positive) and are shifted to the low-frequency range as the temperature decreases. Beyond f_{min}, the NC is practically independent of frequency.

To gain a better insight into the possible reasons for the behaviour of the above shown curves for $\theta(f)$ and $|C|(f)$, we plotted the frequency dependence of the impedance $Z(f)$ for the sample $(Fe_{0.45}Co_{0.45}Zr_{0.10})_{0.42}(PZT)_{0.58}$. As follows from figure 5, the curve $Z(f)$ displays the presence of two maxima. Such behaviour points to the fact that the equivalent circuit of the studied nanocomposites with x around x_{min} includes two resonance *RLC* circuits (at least for frequencies between 100 Hz and 1 MHz), see figure 6. Note also that a similar equivalent circuit was proposed in [9] for the samples of $(Fe_{0.45}Co_{0.45}Zr_{0.10})_x(Al_2O_3)_{1-x}$ with $x < x_C$ deposited in an oxygen-containing atmosphere, where NPs had the 'core–shell' structure. The observed behaviour of $Z(f)$ dependence indicates that each of the two *RLC* circuits has its own resonance frequency:

$$f_{Ri} = \frac{1}{2\pi\sqrt{L_i C_i}}, \qquad (1)$$

where $i = 1$ and 2 are related to the left and right maxima of $Z(f)$ in figure 5. And our estimations show that $Z(f)$ maxima are shifted to higher f as T decreases.

Note also that the presence of two maxima on $Z(f)$ in figure 5 results in variation of the $G(f)$ behaviour from the purely sigmoid-like shape (see the experimental curve in figure 7 and also $G(f)$ curves in figure 2 [24]) against the non-sigmoid-like curves observed for the as-deposited $(Fe_{0.45}Co_{0.45}Zr_{0.10})_x(Al_2O_3)_{(1-x)}$ films (curves 1–3 in figure 5.12 of [38]).

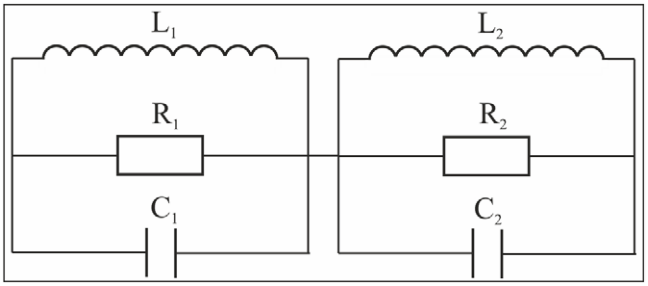

Figure 6. Equivalent circuit describing $Z(f)$ dependence for the as-deposited samples with $0.30 < x < 0.55$ for the frequency range between 100 Hz and 1 MHz.

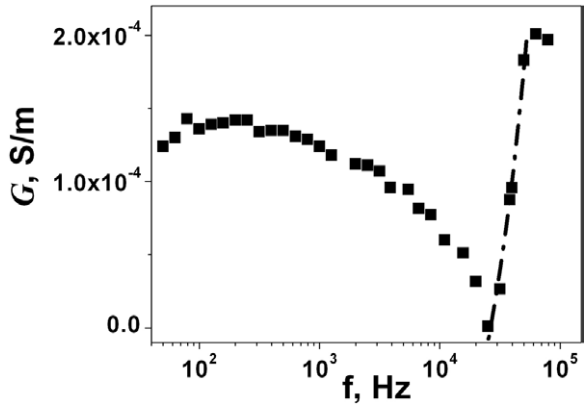

Figure 7. Frequency dependences of the real part of impedance $G(f)$ for the as-deposited sample of $(Fe_{0.45}Co_{0.45}Zr_{0.10})_{0.42}(PZT)_{0.58}$ measured at $T = 303$ K. Points correspond to the experimental data, and the dashed–dotted line is associated with relation (9).

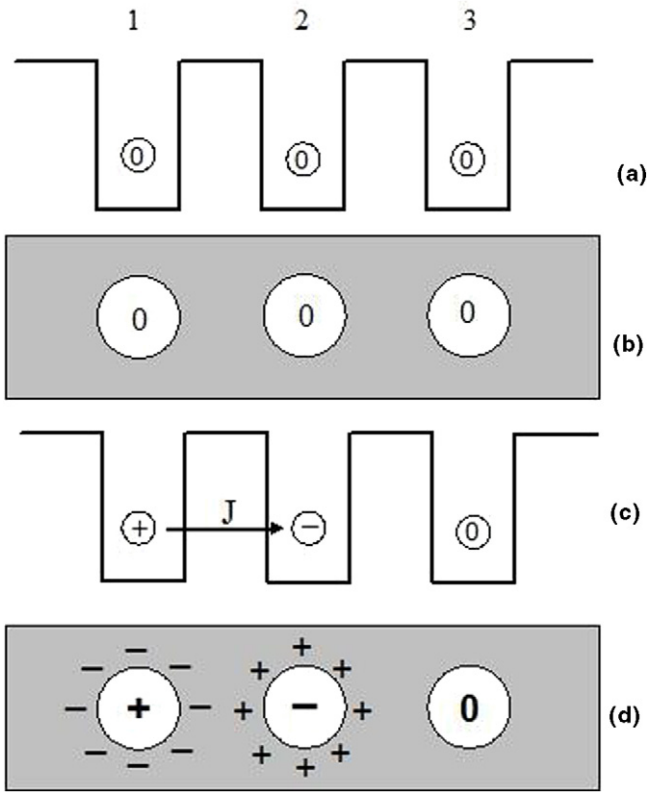

Figure 8. Schematic of potential wells or NPs (*a*), (*c*) in the PZT matrix (*b*), (*d*) before (*a*), (*b*) and after (*c*), (*d*) the electron hopping between wells/NPs under the external alternating electric field E. NPs are shown as white circles and PZT as grey.

As was shown earlier in [7–11] for $(Fe_{0.45}Co_{0.45}Zr_{0.10})_x(Al_2O_3)_{(1-x)}$ nanocomposites, a NC effect was observed only for the films containing NPs with the 'metallic core–oxide shell' structure due to deposition in an Ar + O_2 mixture (see also [25]). In these works we have attributed two resonance *LCR* circuits to the alumina matrix and FeCo-based oxide 'shells'. In the case of $(Fe_{0.45}Co_{0.45}Zr_{0.10})_{0.42}(PZT)_{0.58}$ one can suppose that one of the two resonance *LCR* circuits in figure 6 is due to the influence of the PZT matrix on hopping of the electrons, while the other one should be attributed to fully oxidized NPs.

The curves $|C|(f, T)$, $\theta(f, T)$ and $G(f)$ in figures 3, 4, and 7 for the studied sample of $(Fe_{0.45}Co_{0.45}Zr_{0.10})_{0.42}(PZT)_{0.58}$ (and for other samples around x_{min}) can be explained on the basis of the ac hopping model developed in our previous works [24, 38, 39]. This model takes into account that the electrons in metal–dielectric nanocomposites are localized at the potential wells (in our case, at oxidized NPs embedded in the PZT matrix), figure 8. Without the electric field applied, the potential wells (NPs) arranged with a mean distance a within the PZT matrix are neutral, the electrons jumping from well to well with equal probabilities in all directions (figures 8(*a*) and (*b*)). The probability of every jump in the unit of time $p(T)$ is a function of temperature T, the mean distance a between the wells, dimensions of NPs and the energy of jump activation ΔE_p. The applied external alternating electric field given as

$$E = E_0 \sin \omega t \tag{2}$$

with the circular frequency $\omega = 2\pi f$ is considered to be weak and determining only the direction of jump without a change in the probability $p(x, T, \Delta E_p)$ of the electron jump from one well to another (see, e.g., [40]). Therefore, such a weak field results only in an asymmetry of jumps.

After the application of the first half-period of E, the electron jumps (in time of the Maxwell relaxation τ that is on the order of 10^{-13} s) from the first neutral well (NP) to the second one, and the electric dipole appears between these two charged NPs, figures 8(*c*) and (*d*). When E changes its direction during the next half-period, the electron localized in the second well (NP) should make the next jump back to the first NP (well). But as the charged NPs (due to the trapped or deficient electrons) are surrounded by the ferroelectric PZT matrix, the latter becomes polarized in the vicinity of NPs (see figure 8(*d*)) that leads to an increase in the lifetime τ_m ($\gg \tau$) of the electron captured at the second well (NP)—it cannot return to the first well (NP) during the next half-period of the applied ac field E. So, the formation of a dipole (and polarization of the PZT matrix around NPs) results in the redistribution of the probability density p for the next jump of the electron either backward to the first NP (due to a negative half-period of ac) or forward to the next (third) one. As shown in [24, 38, 39], the total current density of hopping electrons in this process can be given as

$$j = j_0 + j_+ + j_- = GE_0\{\sin \omega t + p \sin[\omega(t - \tau_m)] - (1 - p) \sin[\omega(t - \tau_m)]\}, \tag{3}$$

where t is the running time, j_0 is the first contribution to the electric current during the first half-period of E (due to the first electron jump from the first to the second NP), j_+ is the second contribution to the electric current during the second half-period of E (due to the electron jump from the second to the third NP) and j_- is the third contribution to the electric current if the electron returns to the first well (as against the vector E) with the probability $(1 - p)$ during the second half-period of E.

Since the contributions j_+ and j_- are phase shifted relative to j_0, the total current density j has both real and imaginary parts. The above-mentioned processes causing the ac electron hopping transfer lead to an active component in the alternating current for a parallel equivalent circuit of the nanocomposite sample [24, 38, 39]:

$$j_r = GE_0 \sin \omega t \cdot [1 - \cos \omega \tau_m + 2p \cos \omega \tau_m]. \quad (4)$$

Analysis of relation (4) demonstrates that for low frequencies $j_r(\omega)$ can be given as

$$j_r = j_{LF} = 2pGE_0 \sin \omega t, \quad (5)$$

and at $\omega \to 0$, i.e. for the direct current, an expression for the real part of admittance in (5) is transformed to the following:

$$G_{LF}(\omega \to 0) \approx 2p. \quad (6)$$

In the high-frequency range we have

$$j_r = j_{HF} \cong GE_0 \sin \omega t, \quad (7)$$

and when $\omega = \pi/2\tau_m$, we obtain

$$G_{HF}(\omega \to \infty) \approx 1. \quad (8)$$

For the intermediate region of frequencies (within the limits LF and HF) the active component of the alternating current can be described by the known Mott law [40]:

$$G(f) \approx G_o f^{\alpha}, \quad (9)$$

where G_0 is the coefficient and the exponent α, as differentiated from Mott's model, is dependent on the frequency $\alpha(f)$ [24, 38, 39].

Thus, in accordance with our model [24, 38, 39], in the dielectric regime $G(f)$ dependences for the composites studied should be characterized by the shape approximating the sigmoid-like one and display three characteristic frequency regions: $G_{LF} \approx$ const1, see (6), for low frequencies; $G_{HF} \approx$ const2, see (8), for high frequencies with $G_{HF} > G_{LF}$; and the intermediate region described by relation (9) with frequency-dependent $\alpha = \alpha(f)$, which is represented by the fitted dashed–dotted curve in figure 7. Such a nearly sigmoid-like behaviour of $G(f, T)$ enables one to estimate the values of the probability density p and of the frequency factor α from the developed model and to calculate other parameters that limit the hopping conductance in our case.

To extract $\alpha(f)$, we need to calculate the values of the jump probability p. As was shown in [24, 38, 39], we can calculate p either by direct modelling (using equation (3) or (4), experimental data, and the appropriate fitting procedure) or from experimental $G(f)$ curves (if they are sigmoid-like in character). In fact, a comparison of equations (6) and (8) results in a very simple relation:

$$p \approx \frac{G_{LF}(T)}{2G_{HF}(T)}, \quad (10)$$

making it possible to estimate p values (and then the function $\alpha(f)$) for every temperature T directly from the experimental $G(f)$ curves, where G_{LF} and G_{HF} are experimental values of G at the determined T for low and high frequencies, respectively. This method was used for fitting of $G(f)$ curve in figure 7 at the intermediate frequency range.

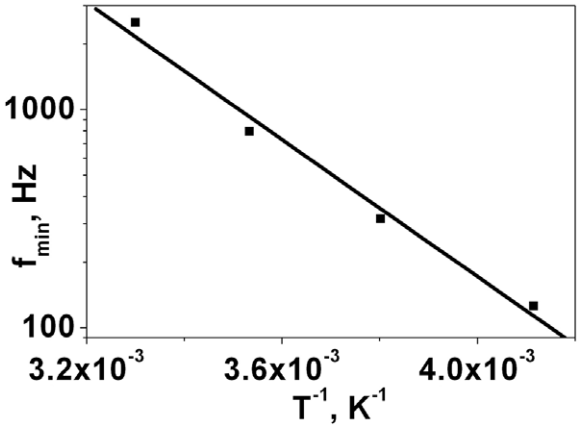

Figure 9. Temperature dependence of f_{min} in relation (10) to the Arrhenius scale for the sample $Fe_{0.45}Co_{0.45}Zr_{0.10})_{0.42}(PZT)_{0.58}$.

The increase in the mean lifetime τ_m of hopping electrons on NPs predicted by our model [24, 38, 39] is determined by the following relation:

$$f \leqslant \frac{1}{2\tau_m} \approx f_{min}, \quad (11)$$

where f_{min} is the frequency at which $\theta(f)$ crosses the abscissa axis in figure 2 or the $|C|(f)$ curve in figure 3 has a minimum.

As established by the developed model [24, 38, 39], the additional polarization observed after the first jump depends on the time τ_m in expressions (3), (4) and (10). This enables one to use relation (10) to extract τ_m from the minima positions of the curves $|C|(f, T)$ in figure 4. Plotting of the function $f_{min}(T)$ on the Arrhenius scale for the sample of $(Fe_{0.45}Co_{0.45}Zr_{0.10})_{0.42}(PZT)_{0.58}$ demonstrates its linearization, see figure 9. Using the slope of this straight line and formulae (10), we can estimate both the activation energy (ΔE_p) of the polarization process (dipole inducing) and the time τ_m of its occurrence (mean lifetime of hopping electrons on NPs) as 300 meV and 10^{-3}–10^{-4} s, respectively.

Therefore, for frequencies $f > f_{min}$ the phase delay $2\pi f \tau_m$ of the next jump either back to the first NP or forward to the third NP under the effect of the external alternating electric field E can become greater than 2π. For large values of τ_m this creates the possibility for positive angles of the phase shift θ and a proper NC (inductive-like contribution) effect in the studied nanocomposites.

4. Conclusions

We have shown that in $(Fe_{0.45}Co_{0.45}Zr_{0.10})_x(PZT)_{(1-x)}$ nanocomposite films deposited in an Ar + O_2 atmosphere a negative capacitance effect (corresponding to predominance of the inductive contribution to admittance) is observed even at room temperature requiring no post-synthesis annealing, different from FeCoZr–Al_2O_3 films. The observed $G(f, T)$ dependences are explained on the basis of a specially developed model for ac hopping conductance of the electrons over oxidized NPs, which are embedded in the PZT matrix. In particular, under the determined conditions such a structure of nanocomposites leads to an increase in the mean lifetime of hopping electrons on NPs and to a delay in the next jump under the external alternating electric field, creating the possibility for positive angles of the phase shift θ and a high NC (inductive-like contribution) effect properly. The activation energy ΔE_p of the polarization process (dipole inducing) and the time τ_m of its occurrence (mean lifetime of the electron on the NP) were estimated as 300 meV and 10^{-3}–10^{-4} s, respectively.

Acknowledgments

The work of the Belarusian group was supported by the Foundation for Polish Science, the VYSBY Program of Swedish Institute, and State Program of Belarus 'Composite materials', Belarusian State program 'Functional materials', projects 1.16 and 1.23.

Dr Eng. Tomasz N Kołtunowicz received a two-year fellowship for outstanding young scientists awarded by the Polish Ministry of Science and Higher Education in 2011.

References

[1] Liu L, Li B, Qin R, Zhao H, Ren X and Su Z 2010 Synthesis and characterization of new bifunctional nanocomposites possessing upconversion and oxygen-sensing properties *Nanotechnology* **21** 285701-7

[2] Margueritat J *et al* 2008 Surface enhanced Raman scattering of silver sensitized cobalt nanoparticles in metal–dielectric nanocomposites *Nanotechnology* **19** 375701-4

[3] Yang T I, Brown R N C, Kempel L C and Kofinas P 2011 Controlled synthesis of core–shell iron–silica nanoparticles and their magneto-dielectric properties in polymer composites *Nanotechnology* **22** 105601–8

[4] Zhu C-L, Chou S-W, He S-F, Liao W-N and Chen C C 2007 Synthesis of core/shell metal oxide/polyaniline nanocomposites and hollow polyaniline capsules *Nanotechnology* **18** 275604–10

[5] Ma H, Jen A K-Y and Dalton L R 2002 Polymer-based optical waveguides: materials, processing, and devices *Adv. Mater.* **14** 1339–65

[6] Stojak K, Pal S, Srikanth H, Morales C, Dewdney J, Weller T and Wang J 2011 Polymer nanocomposites exhibiting magnetically tunable microwave properties *Nanotechnology* **22** 135602-8

[7] Saad A M, Mazanik A V, Kalinin Yu E, Fedotova J A, Fedotov A K, Wrotek S, Sitnikov A V and Svito I A 2004 Structure and electrical properties of CoFeZr–aluminium oxide nanocomposite films *Rev. Adv. Mater. Sci.* **8** 152–7

[8] Saad A, Fedotov A K, Svito I A, Fedotova J A, Andrievsky B V, Kalinin Yu E, Malyutina-Bronskaya V, Patryn A A, Mazanik A V and Sitnikov A 2006 Impedance and magnetization of CoFeZr nanoclusters embedded into alumina matrix *J. Alloys Compounds* **423** 176–80

[9] Fedotova J A, Larkin A, Fedotov A, Kalaev V A, Kalinin Yu E, Sitnikov A, Andrievski B V and Patryn A A 2007 Influence of oxygen on magnetoimpedance of nanocomposites $(Co_{45}Fe_{45}Zr_{10})_X(Al_2O_3)_{100-X}$ *Physics, Chemistry and Application of Nanostructures: Reviews and Short Notes to Nanomeeting-2007* ed V E Borisenko *et al* (Singapore: World Scientific) pp 62–5

[10] Kołtunowicz T N, Żukowski P, Węgierek P, Fedotova J A, Fedotov A K and Larkin A V 2011 Formation of noncoil-like inductance in nanocomposites $(Fe_{0.45}Co_{0.45}Zr_{0.10})_x(Al_2O_3)_{1-x}$ manufactured by ion-beam sputtering of complex targets in Ar+O_2 atmosphere *Acta Phys. Polon.* A **120** 43–5

[11] Fedotova J, Saad A, Larkin A, Fedotova V, Ilyashuk Y, Fedotov A, Kalinin Y and Sitnikov A 2009 Influence of oxygen and nitrogen on impedance and magnetoimpedance of soft magnetic CoFeZr nanoparticles embedded in alumina matrix *9th IEEE Conf. on Nanotechnology IEEE NANO 2009 (Genoa, Italy, 26–30 July 2009)* pp 651–4

[12] Doyle B S 1986 Anomalous low-frequency resonance-type behavior and negative capacitance in doped glasses *J. Phys. D: Appl. Phys.* **19** 1129–40

[13] Ershov M, Liu H C, Li L, Buchanan M, Wasilewsky Z R and Ryzhii V 1997 Unusual capacitance behavior of quantum well infrared photodetectors *Appl. Phys. Lett.* **70** 1828–30

[14] Chen N C, Wang P Y and Chen J F 1998 Low frequency negative capacitance behavior of molecular beam epitaxial GaAs *n*-low temperature-*i*-*p* structure with low temperature layer grown at a low temperature *Appl. Phys. Lett.* **72** 1081–3

[15] Perera A G U, Shen W Z, Ershov M, Liu H C, Buchanan M and Schaff W J 1999 Negative capacitance of GaAs homojunction far-infrared detectors *Appl. Phys. Lett.* **74** 3167–9

[16] Ilyas M, Zulfequar M and Husain M 1999 Anomalous dielectric behaviour in a-Ga_xTe_{100-x} alloys ($0 \leqslant x \leqslant 10$) *Physica* B **271** 125–35

[17] Lemmi F and Johnson N M 1999 Negative capacitance in forward biased hydrogenated amorphous silicon p^+–i–n^+ diodes *Appl. Phys. Lett.* **74** 251–3

[18] Ershov M, Liu H C, Li L, Buchanan M, Wasilewski Z and Jonscher A 1998 Negative capacitance effect in semiconductor devices *IEEE Trans. Electron Devices* **45** 2196–206

[19] Kwok H L 2003 Modeling negative capacitance effect in organic polymers *Solid-State Electron.* **47** 1089–93

[20] Kwok H L 2008 Understanding negative capacitance effect using an equivalent resistor–capacitor circuit *Phys. Status Solidi* c **5** 638–40

[21] Bakueva L, Konstantatos G, Musikhin S, Ruda H E and Shika A 2004 Negative capacitance in polymer–nanocrystal composites *Appl. Phys. Lett.* **85** 3567–9

[22] Berlab S and Brutting W 2002 Dispersive electron transport in tris(8-hydroxyquinoline) aluminum (Alq_3) probed by impedance spectroscopy *Phys. Rev. Lett.* **89** 286601

[23] Żukowski P, Kołtunowicz T N, Węgierek P, Fedotov A, Fedotova J and Larkin A 2011 Sposób wytwarzania bezuzwojeniowych indukcyjności do układów mikroelektronicznych Patent claim n. P 390789 22.03.2010 *Biuletyn Urzędu Patentowego* **20** 35

[24] Kołtunowicz T N, Żukowski P, Fedotova V V, Saad A M and Fedotov A K 2011 Hopping conductance in nanocomposites $(Fe_{0.45}Co_{0.45}Zr_{0.10})_x(Al_2O_3)_{1-x}$ manufactured by ion-beam sputtering of complex target in Ar+O_2 ambient *Acta Phys. Polon.* A **120** 39–42

[25] Fedotova J, Przewoznik J, Kapusta C, Milosavljević M, Kasiuk J V, Zukrowski P, Sikora M, Maximenko A A,

Szepietowska D and Homewood K P 2011 Magnetoresistance in FeCoZr–Al_2O_3 nanocomposite films containing 'metal core–oxide shell' nanogranules *J. Phys. D: Appl. Phys.* **44** 495001

[26] Kasiuk J V, Fedotova J A, Marszalek M, Karczmarska A, Mitura-Nowak M, Kalinin Yu E and Sitnikov A V 2012 Effect of oxygen pressure on phase composition and magnetic structure of FeCoZr–Pb(ZrTi)O_3 nanocomposites *Phys. Solid State* **54** 178–84

[27] Fedotova J, Kasiuk Yu, Larkin A, Przewoznik J, Kapusta Cz and Kalinin Yu 2009 Structure and resistivity of FeCoZr-dielectric granular nanocomposites sinterd in mixed Ar+O atmosphere *Proc. 54th Internationales Wissenschaftliches Kolloquium—Information Technology and Electrical Engineering—Devices and Systems, Materials and Technology for the Future (54-IWK) (Ilmenau, Germany, 7–10 September 2009)* ISBN 973-1-938843-45-1

[28] Fedotova J, Koltunowicz T N and Żukowski P 2012 Transport ładunków i właściwości strukturalne wybranych nanokompozytów metal-dielektryk *Politechnika Lubelska, Lublin* 173pp (in Polish)

[29] Stauffer D and Aharony A 2003 *Introduction to Percolation Theory* (London: Taylor and Francis)

[30] Saad A M *et al* 2006 Characterization of $(Co_{0.45}Fe_{0.45}Zr_{0.10})_x(Al_2O_3)_{1-x}$ nanocomposite films applicable as spintronic materials *Phys. Status Solidi* c **3** 1283–90

[31] Narendra Babu S, Bhimasankaram T and Suryanarayana S V 2005 Magnetoelectric effect in metal–PZT laminates *Bull. Mater. Sci.* **28** 419–22

[32] Nan C W, Bichurin M I, Dong Sh, Viehland D and Srinivason G 2008 Multiferroic magnetoelectric composites: historical perspective, status, and future directions *J. Appl. Phys.* **103** 031101

[33] Bracke L P M and Van Vliet R G 1981 A broadband magneto-electric transducer using a composite material *Int. J. Electron.* **51** 255–62

[34] Kołtunowicz T 2007 Station to testing temperature and frequency dependence of electrophysical properties of semiconductors exposed to implantation *Elektronika—Konstrukcje, Technologie, Zastosowania* **48** 37–40 (in Polish)

[35] Kołtunowicz T N 2011 Measuring stand for testing electrical properties of nanocomposites—determination of the measurement uncertainty budget *Meas. Autom. Monit. (PAK)* **57** 694–6 (in Polish)

[36] Andriyevski B, Patryn A, Czapla Z, Dacko S, Fedotova J A, Larkin A V and Fedotova V V 2008 Impedance spectroscopy study of amorphous composites $x(Fe_{0.45}Co_{0.45}Zr_{0.10})+(1-x)(Al_2O_3)$ *Prz. Elektrotech.* **84** 117–9

[37] Larkin A V, Fedotov A K, Fedotova J A, Koltunowicz T N and Żukowski P 2012 Temperature and frequency dependences of impedance real part in the FeCoZr-doped PZT nanogranular composites *Mater. Sci.—Poland* **30** 75–81

[38] Żukowski P, Kołtunowicz T, Partyka J, Fedotova Yu A and Larkin A V 2009 Hopping conductivity of metal–dielectric nanocomposites produced by means of magnetron sputtering with the application of oxygen and argon ions *Vacuum* **83** S280–3

[39] Żukowski P, Kołtunowicz T, Partyka J, Węgierek P, Kolasik M, Larkin A V, Fedotova J A, Fedotov A K, Komarov F F and Vlasukova L A 2008 A model of hopping recharging and its verification for nanostructures formed by the ion techniques *Prz. Elektrotech.* **84** 247–9 (in Polish)

[40] Mott N F and Davis E A 1979 *Electron Process in Non-Crystalline Materials* (Oxford: Clarendon)